Aptamer-based monitoring of drug uptake into cells and vertebrates

AUTHORS

Eiman A. Osman[1], Thomas P. Rynes[2], Lucia Wang[3], Karen Mruk[2] and Maureen McKeague[*1,3]

[1]Department of Chemistry, Faculty of Science, McGill University, Montreal, QC H3A 0B8, Canada

[2]Department of Pharmacology and Toxicology, Brody School of Medicine, East Carolina University, Greenville, NC 27834, US

[3]Pharmacology and Therapeutics, Faculty of Medicine, McGill University, Montreal, QC H3G 1Y6, Canada

* Correspondence should be addressed: Email: maureen.mckeague@mcgill.ca

GRAPHICAL ABSTRACT

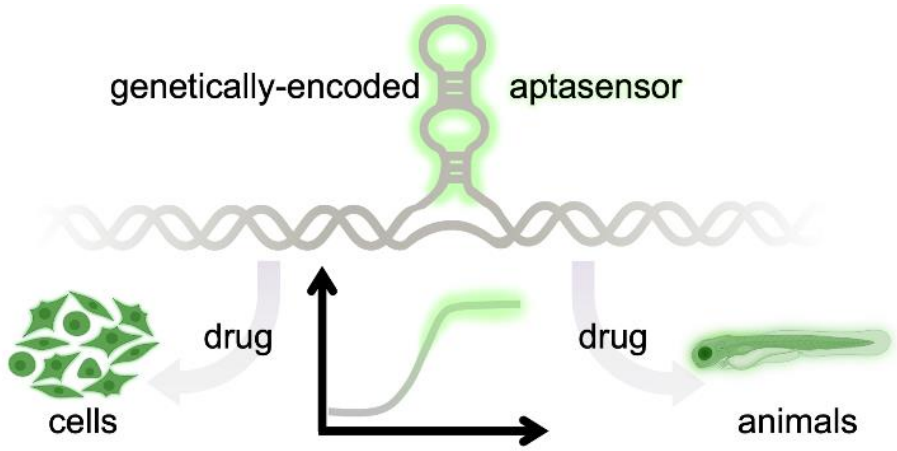

SYNOPSIS: We developed a genetically-encoded aptamer biosensor platform for non-invasive real-time measurement of drug uptake in cells and whole animals.

ABSTRACT

Sensing small molecules, including drugs and their metabolites inside cells, is critical for drug discovery and development, diagnostics, and precision medicine. To facilitate sensitive, long-term studies of drug uptake in cultured cells and animals, we developed a genetically-encoded aptamer biosensor platform for non-invasive real-time measurements of drug distribution. We combined the high specificity of aptamer molecular recognition with the easy-to-detect properties of fluorescent proteins. We tested six different aptamer biosensors, showcasing the platform versatility. The biosensors display high sensitivity and specificity for detecting their specific drug target over related analogs. Furthermore, the biosensor responses were dose dependent and could be detected in individual live cells. We designed our platform for easy integration into animal genomes; thus, we incorporated one aptamer biosensor into zebrafish, an important model vertebrate. The biosensor was stably expressed and enabled non-invasive drug biodistribution imaging in whole animals across different timepoints. To our knowledge, this is the first example of an integrated aptamer biosensor encoded by a vertebrate animal. As such, our aptamer encoded biosensors address the need for non-invasive whole animal biosensing ideal for pharmacokinetic-pharmacodynamic analyses that can be expanded to detect diverse molecules of interest. Furthermore, due to the lack of species-specific machinery, our biosensors can be potentially adapted for any model organism of interest.

INTRODUCTION

Uptake, transportation, efflux, and the concentration of drugs inside cells is crucial for exploring pharmacokinetics and characterizing drug efficacy, targeting, toxicity, and mechanisms of drug resistance.[1, 2] Technologies that enable rapid detection of drugs and their metabolites inside individual cells can improve drug delivery and optimization, thus enhancing therapeutic outcomes, and minimizing adverse effects.[3, 4] However, interrogating molecules and processes inside cells is challenging. Typically, instrument-based analytical methods, including high pressure liquid chromatography,[5] mass spectrometry (MS),[6-8] and magnetic resonance imaging[9] are used to measure drugs and their metabolites. Recently, quantitative measurement of therapeutics in cancer models has been demonstrated using instrumentation such as MALDI-MS.[10] In all of these cases, cells and tissues must be lysed[11, 12] or embedded, frozen, and cross sectioned, thus precluding real-time cellular measurements[13] and non-invasive animal studies,[14] thereby limiting studies to bulk cellular populations.[15, 16]

Confocal microscopy, two photon microscopy, near infrared imaging, and positron emission tomography, on the other hand, have been extremely valuable for non-invasive and real-time monitoring of biomolecules,[17] cellular processes,[18, 19] and tissue patterning.[20, 21] Indeed, using fluorescent dyes and probes, imaging has enabled the study of oxidative stress[22] and lipid membrane organization in whole organisms[23], characterization of in vivo biodistribution properties of drug delivery vehicles,[24] longitudinal monitoring of inflammation in animals,[25] tracking of cellular growth and apoptosis,[26, 27] and recording of brain circuitry activity.[28] Furthermore, with the development of high-throughput imaging platforms and imaging analysis software, semi-quantification is possible.[29, 30] However, sensing small molecules including drugs and their metabolites remains a challenge due to the lack of suitable probes with specific molecular recognition properties.

An important approach to improve the specificity and real-time detection of molecules inside cells includes the use of fluorescent biosensors, incorporating either small molecule probes or genetically-

encoded fluorescent proteins.[31-37] The development of biosensors requires two essential components: 1) a molecular recognition agent that specifically detects the target of interest and 2) a reporter to transduce the detection into a measurable signal. Indeed, a long list of genetically encoded biosensors[31] making use of single-fluorescent protein approaches, fluorescence resonance energy transfer (FRET),[38] or bioluminescence resonance energy transfer (BRET),[39] have been developed to sense metal ions such as Ca^{2+},[40] and K^{+} [41] redox species,[42] glucose,[43] neurotransmitters,[44] amino acids,[45] and nucleotides.[46] Recently, a FRET-based encoded biosensor was developed to sense the uptake of sulphonamide diuretic drugs. Here, the drug's target protein and a ligand were conjugated to a pair of FRET proteins such that, in the absence of the drug, the encoded ligand occupied the target protein binding site, bringing the FRET pairs into sufficient proximity for a strong FRET signal. However, upon accumulation of sufficiently high concentrations of the drug in the cytosol, the ligand was displaced, resulting in a decreased FRET signal.[32] This study highlighted the utility of monitoring drug uptake in live cells and the promise of protein-based genetic biosensors. However, the complexity of modifying promoters and proteins to detect different targets is challenging and thus has prevented the broad application and development of genetically encoded biosensors for monitoring a wide range of small molecule drugs.[47] Additionally, biosensors designed using proteins often rely on protein function that is specific to a species, making them unsuitable for use in diverse cell and animal models.[48]

Aptamers offer a versatile solution for biosensing,[49, 50] enabling the identification of various small molecules including drugs, toxicants,[51] toxins,[52] metabolites,[53] and even ions.[54] Aptamers are short, single-stranded nucleic acids that selectively bind to their targets. They can be identified through an in vitro selection process called SELEX (Systematic Evolution of Ligands by Exponential Enrichment),[55-57] which involves iterative rounds of selection and amplification to identify sequences with high affinity and specificity for the desired target. The key features that render aptamers preferable to other selective molecules such as antibodies and promoters are their versatility, reproducibility, and low immunigencity.[58-65]

Here, to enable sensitive and long-term studies of drug cellular uptake into cultured cells and animals, we integrated the specificity of aptamers that target small molecule drugs with the enhanced fluorescence of green fluorescent protein (GFP). Our biosensor platform is genetically encoded, enabling straightforward integration into the genomes of cells and animals. We show that the encoded RNA aptamers enable specific imaging and relative quantitation of drug uptake in mammalian cells. We applied our biosensor design to a panel of six different aptamer biosensors demonstrating the generalizability of the approach. Finally, we integrated the aptamer biosensors into the genome of the vertebrate model zebrafish. We show that our genetically encoded aptamer biosensor enables live imaging of drug biodistribution throughout the lifespan of a vertebrate. In summary, we developed an aptamer biosensor that allows for non-invasive, real-time, and single cell measurements of drug distribution.

RESULTS AND DISCUSSION

Developing a genetically encoded aptamer biosensor platform for cells and zebrafish

Our genetically encoded aptamer biosensor platform makes use of an aptamer-ribozyme construct that is active in yeast and mammalian cells.[66-68] In our system, binding of the aptamer's target activates expression of green fluorescent protein (GFP). RNA aptamers are inserted into the loops of a self-cleaving ribozyme,[69-72] such that ribozyme activity is maintained. In this way, when the aptamer-

ribozyme construct is encoded in the 3'-UTR of GFP, the GFP mRNA is cleaved and degraded, resulting in the absence of GFP fluorescence. However, when the aptamer's target binds to the aptamer, it blocks the tertiary interactions necessary for ribozyme activity. As a result, the GFP mRNA is stabilized by the polyA tail and is effectively translated into the fluorescent protein. Given that GFP synthesis is dependent on the concentration of the small molecule, we hypothesized that this platform would be useful for intracellular biosensing, where any aptamer could theoretically be used to specifically recognize a target-of-interest. This platform is termed "**D**NA **I**ntegrated **V**ersatile **E**ncoded-Aptamer biosensors" (DIVE aptasensors, **Scheme 1**).

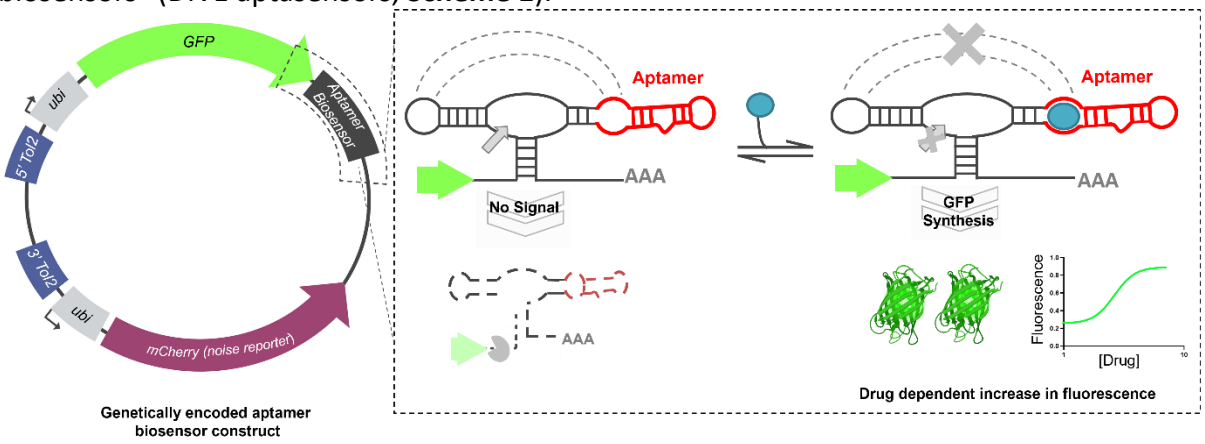

Scheme 1. **DNA Integrated Versatile Encoded-Aptamer biosensor (DIVE aptasensor) platform.** The DNA plasmid encodes the RNA aptamer biosensor and two fluorescent reporter genes. GFP is directly coupled to the aptamer biosensor and mCherry acts as a noise control. Ubiquitous (ubi) promoters control both genes, enabling constitutive expression in zebrafish. Tol2 arms are available for integrating the plasmid into the zebrafish genome. The aptamer biosensor detects the presence of drug, enabling GFP synthesis and a detectable signal. In the absence of the drug, the GFP gene is degraded and there is no measurable green fluorescence.

For generating a highly robust biosensing signal, we included two gene reporters: GFP acting as the biosensing transducer coupled to the aptamer sensor platform; and mCherry is constituently expressed from the same plasmid (**Scheme 1**). All GFP measurements are therefore normalized to mCherry, accounting for cell death/toxicity, varying concentrations of the transfected biosensor platform, and cell-cell variations in gene expression.[73] Given that our ultimate goal is to develop genetically encoded biosensors that function across cell types and in a vertebrate model, we developed a custom plasmid suitable for zebrafish and mammalian cells (**Scheme 1, Figure S1**). Specifically, GFP and mCherry are controlled by the constitutive ubiquitous (ubi) promoter[74] that is active throughout zebrafish development. Furthermore, the plasmid contains 5' and 3' Tol2 transposable elements to facilitate genome integration in zebrafish.[75] An important feature of our biosensor system is that the fluorescent proteins chosen for the mammalian screen are the same as those that are used in zebrafish without codon optimization. In this way, the sequence context of the biosensor, which is encoded between GFP and the polyA tail, remains constant and minimizes differences between mammalian cell and zebrafish biosensing.

Given that cellular biosensing is inherently noisy,[73, 76] we first wanted to establish suitable negative and positive controls for our DIVE biosensing platform. We therefore cloned controls lacking the aptamer sensing modules. Specifically, we produced an "always OFF" biosensor (negative control) composed of an active self-cleaving ribozyme, and an "always ON" biosensor (positive control) composed of an

altered ribozyme that lacked self-cleavage activity and therefore did not interfere with GFP expression. For every measurement, we measured the GFP/mCherry ratio. As expected, the "always OFF" biosensor resulted in very low GFP fluorescence relative to mCherry whereas the "always ON" biosensor resulted in high GFP fluorescence, resulting in GFP/mCherry ratios of 0.5 and 3.4, respectively. Notably, the "always ON" biosensor gave the same measured fluorescent ratios as the core plasmid containing only GFP and mCherry (ratio = 3.6). Furthermore, the "always OFF" biosensor resulted in higher GFP signal compared to the background fluorescence measured in the cells. However, when normalized to the background mCherry signal, the relative ratios of GFP/mCherry for the "always OFF" biosensor were comparable to the non-transfected cells (ratio of 0.7) (**Figure 1**). These controls established the upper and lower limits for potential biosensing dynamic range.

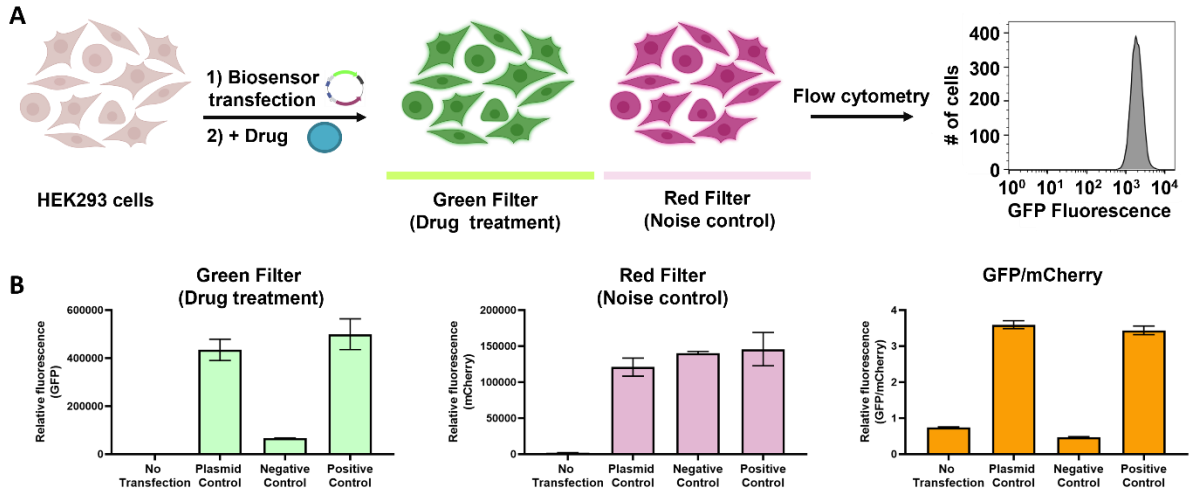

Figure 1. **Testing the DIVE biosensing platform controls in HEK293T cells.** (A) Workflow of the assay. (B) Fluorescence measurements for each control: no transfection, the core plasmid containing only GFP and mCherry, the "always OFF" negative control, and "always ON" positive control. GFP and mCherry fluorescence is measured for each cell population. The relative GFP/mCherry ratio is then calculated and plotted. Data are the mean and standard deviation of triplicates.

DIVE aptasensors for six pharmaceutical drugs

With the appropriate controls in hand, we next compared biosensor activity for six small molecule pharmaceuticals with diverse structures (**Figure S2**) and functions. Theophylline is a bronchodilator used for respiratory disorders; folinic acid is a folate derivative used for decreasing the toxicity of anticancer drugs in healthy cells; gardiquimod is an experimental drug and toll-like receptor (TLR) agonist that modulates the immune system; aciclovir is an antiviral medication and nucleoside analog; and neomycin and tetracyclines are antibiotics. Importantly, protein-based encoded biosensors have not been reported for these molecules with the exception for tetracycline and thus our developed DIVE biosensors dramatically increase the number of drugs that can be monitored within cells.

Aptamer-ribozyme constructs adapted from yeast or mammalian cells[77-79] were chosen for each of our six drugs and incorporated into our DIVE plasmid to generate six individual genetic biosensor platforms. Each DIVE aptasensor was transfected into HEK293T cells. We then incubated the cells with each drug and performed a preliminary comparison of DIVE aptasensor activity following 72 h of drug uptake via flow cytometry (**Figure S3**). In each case, we also included positive and negative controls. All six

biosensors resulted in an increase in the relative GFP/mCherry ratio in the presence of the appropriate target drug, confirming the function of the genetically encoded platform in mammalian cells (**Figure 2**). Furthermore, our single-cell measurements by flow cytometry were consistent with bulk measurements (**Figure S4**). The **DIVE_theo** sensor showed the highest response, with a 3.8-fold increase in fluorescence as compared to in the absence of the drug. **DIVE_gard**, **DIVE_acic**, and **DIVE_FA** biosensors resulted in up to a 1.9-fold increase in fluorescence as compared to the absence of drug. Interestingly, except for the theophylline aptamer, each of the aptamers employed in the biosensors bind to their drug targets with nanomolar dissociation constants under physiological magnesium concentrations (0.5 mM)[79](**Figure S5**). In contrast, the theophylline aptamer, which resulted in the best biosensor response, displays strong magnesium dependence, resulting in substantially weaker micromolar binding (K_D = 5 ± 2 µM) at 0.5 mM Mg^{2+} measured using a surface plasmon resonance assay (**Figure S5**). Therefore, the difference in responses measured by our biosensors is not due to aptamer affinity but rather reflect drug uptake into cells. Indeed, it is known that aminoglycosides and other antibiotics have poor cellular uptake into mammalian cells,[80] consistent with the low "turn-on" fluorescence measured. Furthermore, folinic acid is a negative charged molecule that requires specific membrane transporters for its transport in and out of the cell. HEK293T cells express these transporters[81] but tightly regulate the uptake, corresponding to the small but statistically significant measured biosensor response. Indeed, previous reports demonstrate improved uptake of folinic acid upon overexpressing the human folate transporter *SLC46A1*.[79] Taken together, our results demonstrate that the DIVE aptasensors enable single cell measurement of drug uptake.

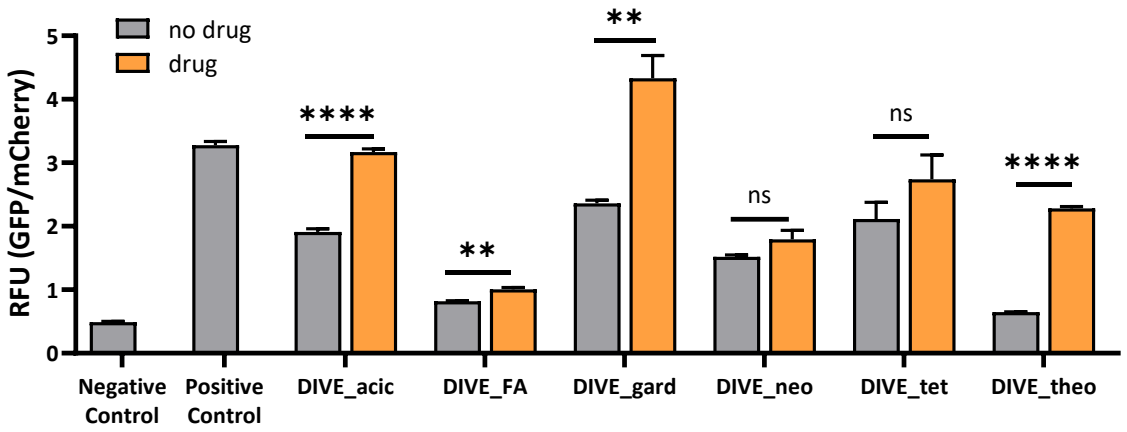

Figure 2. **Comparison of DIVE aptasensors for six drugs.** GFP/mCherry ratio for each DIVE aptasensor in HEK293T cells in the presence and absence of its corresponding drug: DIVE_acic with aciclovir at 100 µM; DIVE_FA with folinic acid at 1 mM; DIVE_gard with gardiquimod at 50 µM; DIVE_neo with neomycin at 2 mM; DIVE_tet with tetracycline at 500 µM; and DIVE_theo with theophylline at 1 mM. Data are the mean and standard deviation of triplicates. p values from a two-tailed, unpaired t-test with Welch's correction are indicated. Significance summary: $p > 0.05$(ns), $p \leq 0.01$(**), $p \leq 0.0001$(****).

DIVE aptasensors show a dose response relationship and distinguish their target drugs from analogs

Given that the DIVE_theo and DIVE_gard biosensors showed the highest response when incubated with their target drug, we next performed a dose-response study. As the nominal drug concentration was increased, the relative GFP also increased. Data were fit to a dose response curve, resulting in half maximal effective concentrations (EC_{50}) of 257 µM (R^2 = 0.9928) for DIVE_theo and 1.3 µM (R^2 = 0.9242) for DIVE_gard. Data were also fit using a simple linear regression establishing a linear dynamic range for

the DIVE_theo biosensor of 8 and 320 µM and a limit of detection (LOD) of 7.5 µM (**Figure 3A**). For the DIVE_gard biosensor, the linear dynamic range based on the nominal dose extended to 3 µM; however, due to the high background expression of this biosensor, the LOD was approximately 1 µM (**Figure 3B**). These results confirm that our encoded-aptamer biosensors enable the detection of drug uptake into cells in a dose-dependent manner. Given that dose-response studies are essential in drug research and development, providing critical information regarding safety and dosing,[82] our biosensors may be useful for monitoring drug uptake in engineered cells or drugs encapsulated into delivery vehicles.

Specificity is critical in drug development to avoid negative side effects and toxicity.[83, 84] We therefore wanted to ensure that the aptamers maintained their specificity for their targets within the DIVE biosensing platform. Specifically, we compared biosensor activity in response to analogs of their target drugs. For the DIVE_theo biosensor we incubated cells separately with high concentrations of caffeine which differs from theophylline by a single methyl group. Importantly, the DIVE_theo biosensor showed almost no activity in the presence of caffeine. Even at 1 mM concentrations, the biosensor activity with caffeine was comparable to background levels, highlighting its specificity (**Figure 3C**). For the DIVE_gard biosensor, we examined the specificity against the analog resiquimod in which an ether replaces the secondary amine in gardiquimod. Again, our DIVE aptasensor showed almost no activity in the presence of resiquimod, illustrating a high degree of specificity (**Figure 3D**).

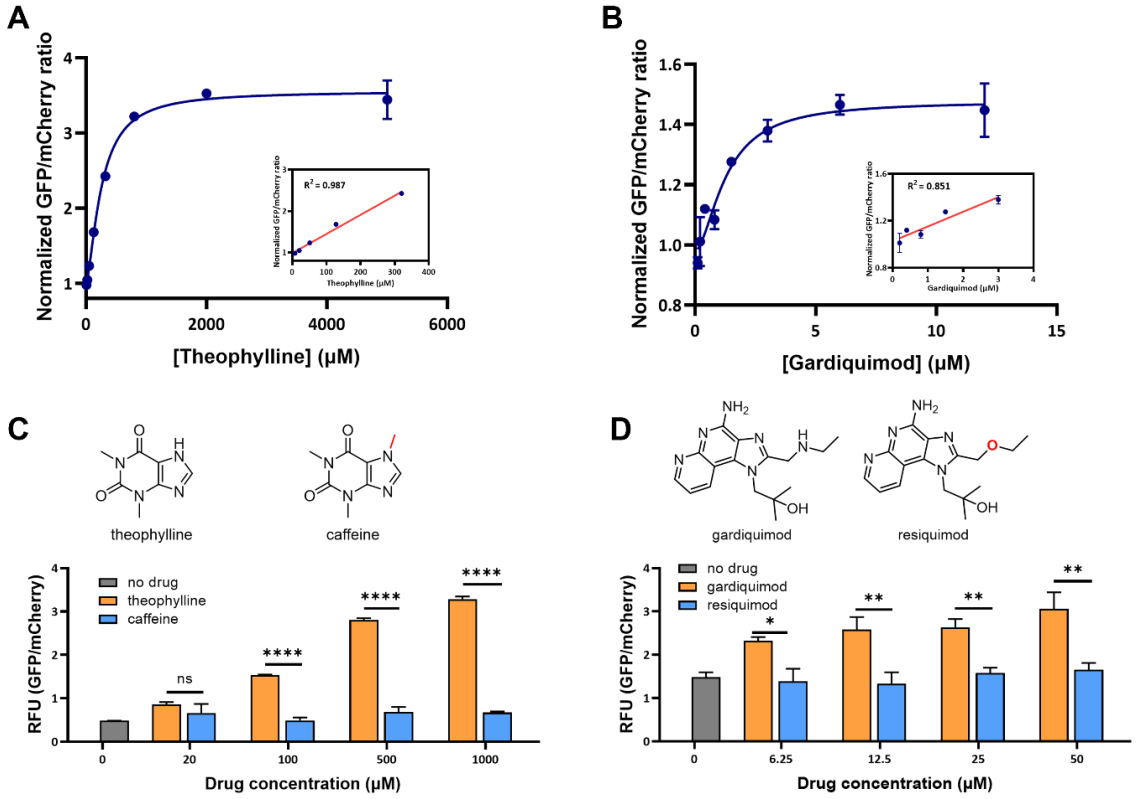

Figure 3. **DIVE aptasensor performance: dose response and specificity.** Normalized fluorescence intensity of GFP/mCherry ratios after incubating HEK293T cells with increasing concentrations of their corresponding drugs (A) DIVE_theo. (B) DIVE_gard. Insets: linear dynamic range for each biosensor. (C) DIVE_theo biosensor specificity in the presence of theophylline and caffeine. (D) DIVE_gard biosensor specificity in the presence of gardiquimod and resiquimod. Data are the mean and standard deviation of triplicates. p values from a 2-way ANOVA with Šídák's multiple comparisons test indicated. Significance summary: $p > 0.05$(ns), $p \leq 0.05$(*), $p \leq 0.01$(**), $p \leq 0.0001$(****).

Live cell imaging of biosensor activity in HEK293T cells

Towards our long-term goal of non-invasive drug monitoring, we next determined whether our DIVE aptasensors would be suitable for live-cell imaging. We therefore evaluated the theophylline biosensor in live HEK293T cells and compared the results to the negative and positive controls described earlier. Cells containing DIVE_theo were treated with various concentrations of theophylline and caffeine. Without any fixing or mounting, we directly imaged the cells in the well plates for both green and red fluorescence. As expected, the red filter showed red fluorescence in all cell conditions since mCherry is constitutively expressed. The positive control "always ON" platform displayed bright green fluorescence, whereas the negative control "always OFF" platform showed no green fluorescence (**Figure 4A**). Excitingly, cells harboring our DIVE_theo biosensor treated with 0.5- and 1-mM theophylline displayed bright green signals (**Figure 4C**) and almost no signals were observed in the absence of theophylline or those treated with caffeine (**Figure 4B** and **S6**). Our live cell imaging results are comparable to the flow cytometry measurements, thus confirming the robustness of our aptamer biosensors for noninvasive live cell imaging of drug uptake.

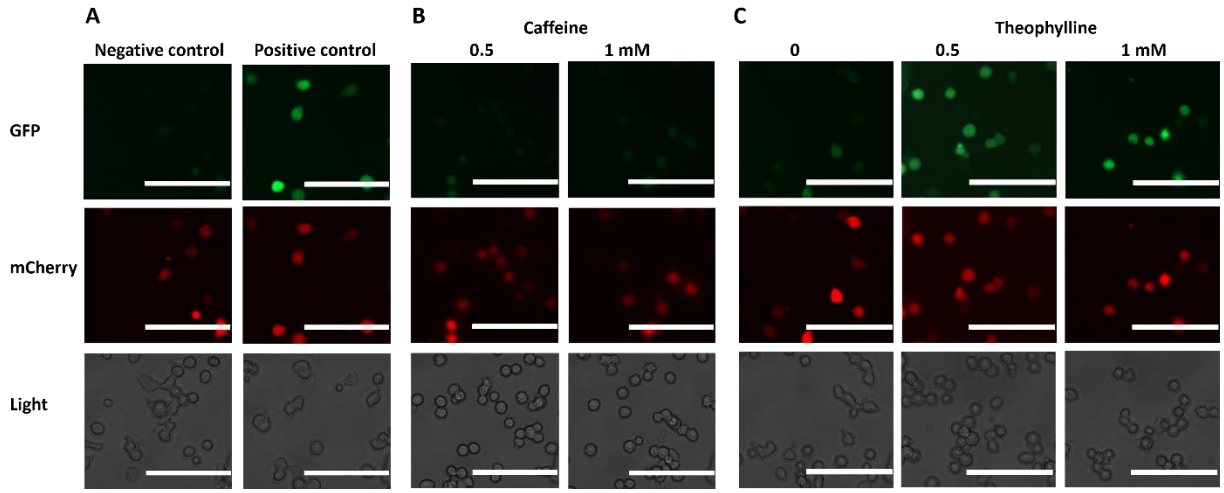

Figure 4. **Live cell imaging of drug uptake using DIVE aptasensors.** (A) HEK293T cells expressing the "always OFF" and "always ON" controls. (B) HEK293T cells expressing DIVE_theo and treated with caffeine. (C) HEK293T cells expressing the DIVE_theo biosensor treated with theophylline. Scale bars: 100 µm.

Non-invasive cellular biosensing of theophylline in a vertebrate model

Since our aptamer-based biosensors enabled live cell detection of drug uptake in mammalian cells, we sought to assess their biosensing capabilities in a whole vertebrate animal model. Zebrafish have emerged as a powerful preclinical model for human disease and, importantly, respond to small molecules and drug treatments at physiologically relevant doses.[85] We therefore examined the function of DIVE_theo in zebrafish. The biosensors and controls were integrated into the zebrafish genome using Tol2-mediated transgenesis.[75, 86] Fish were raised to adulthood and resulting F2 embryos expressing the biosensors were used for experiments (**Figure 5A**). We performed all experiments using 1 mM theophylline since zebrafish exhibited toxicity effects at higher drug concentrations (**Figure S7**), consistent with theophylline dosing studies in patients[87] .

Transgenic embryos at 24 hours post fertilization (hpf) expressing DIVE_theo were bathed in media in the absence and presence of theophylline. Imaging of individual embryos revealed a small observable green fluorescence in the treated fish after as little as four hours, with a marked increase in green

fluorescence after 24 h (**Figure 5B**). In comparison, there was no change in green fluorescence in the fish that were not bathed in theophylline. In contrast, the "always ON" positive control biosensor was not impacted by theophylline treatment, confirming that the green signal resulted from DIVE_theo detecting theophylline drug uptake (**Figure S8**). By quantifying the fluorescent signals, the animals treated with 1 mM theophylline 24 hpf showed a 5.9-fold increase in signal as compared to fish that did not receive the drug (**Figure 5C**). This value is comparable to the 3.8-fold signal generated in mammalian cells with 1 mM theophylline. The improved signal measured in zebrafish as compared to mammalian cells likely results from the stable integration of the biosensor into the genome as compared to the transient transfection performed in HEK293T cells. Together these results suggest that HEK293T cells can serve as a biosensing prototyping platform[88] for developing new DIVE aptasensors that function in zebrafish. Given the short time (days) to test biosensors in mammalians cells compared to (weeks-months) in zebrafish, this would greatly enable the development of new zebrafish biosensing tools.

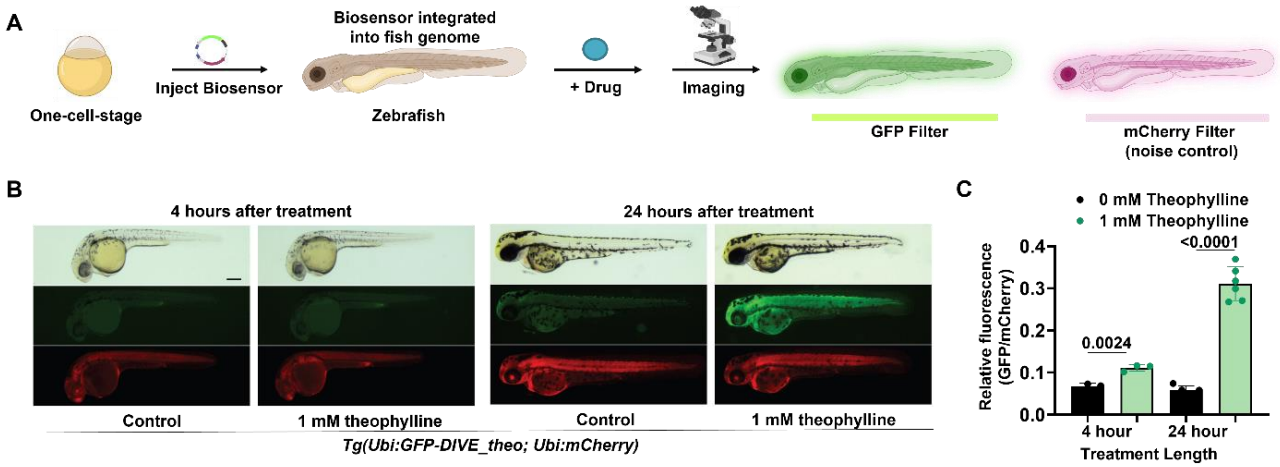

Figure 5. Noninvasive imaging of drug uptake in zebrafish using DIVE aptasensors. (A) Workflow for generating zebrafish expressing the DIVE aptasensors. (B) Representative brightfield and fluorescent micrographs from 24 hpf embryos containing the integrated biosensor plasmid *(Ubi:GFP-DIVE_theo; Ubi:mCherry).* Embryos were bathed in 1 mM theophylline beginning at 24 hpf then imaged at 4 h and 24 h after theophylline treatment. Zebrafish orientation is lateral view, anterior left. Scale bar: 250 µm. (C) Quantification of pixel intensity of GFP and mCherry was calculated for the trunk of the zebrafish and the GFP/mCherry ratio plotted. The average GFP/mCherry ratio ± s.d. with values for individual fish shown. p values from a two-tailed, unpaired t-test with Welch's correction are indicated.

We anticipate that our encoded aptamer biosensors will be valuable across multiple disciplines that study and monitor drug uptake under different conditions. For example, these biosensors can be used for comparing uptake dynamics from different drug formulations, or to compare tissue specificity. Furthermore, drug uptake can be directly compared to animal behavior due to the live and noninvasive nature of these biosensors and therefore will enhance small molecule studies relevant to animal behavior and development. On the other hand, from an environmental perspective, our biosensors can be used to compare the fate, transformations, and uptake of drugs under different environmental conditions.[89] For example, it has been shown that small changes in water pH alter uptake of common pharmaceuticals in fish[90,89].

Our aptamer biosensors are unique in that they can be stably integrated into animal cells and persist through the lifetime and multiple generations of zebrafish. Though aptamers have been developed into numerous biosensing platforms due to their high affinity and ability to undergo conformational changes

in response to specific target molecules, we addressed a major challenge in noninvasive live cell biosensing by coupling the binding properties of RNA aptamers to catalytic RNA. Light-up RNA aptamers including Mango[91] and Broccoli[92] can also be engineered and encoded into whole animals and may result in faster response rates, but the light-up aptamer dyes are expected to exhibit irregular distributions across the animal, hence complicating precise drug uptake monitoring. Here, we focused on the detection of pharmaceuticals; however, there are thousands of reported aptamers to a wide range of xenobiotics and endogenous molecules including metal ions, toxins, toxicants, lipids, and proteins. As such, our DIVE biosensing platform can be theoretically expanded to detect nearly any molecule that accumulates in the cytosol, enabling live cell imaging or noninvasive whole animal monitoring for a plethora of applications.

CONCLUSION

In conclusion, we developed genetically encoded aptamer biosensors suitable for use in mammalian cells and zebrafish representing the first example of an encoded aptamer sensor in a transgeneic vertebrate. We compared different aptamer-based biosensors to a panel of pharmaceuticals, with theophylline and gardiquimod biosensors showing the best sensitivity and specificity. Our biosensors enabled single-cell monitoring of drug uptake in live cells in a dose-response manner. We further applied our biosensors to zebrafish, resulting in robust and precise detection of theophylline at various timepoints. We anticipate that these biosensors will be useful for a range of applications, from environmental toxicity monitoring to studying drug pharmacokinetics and formulation.

METHODS

Reagents and small molecule drugs

All reagents were obtained from commercial suppliers and used without further purification. Oligonucleotides were purchased from IDT without further purification (Coralville, IA, USA). Aciclovir (A4669), Gardiquimod (cat# SML0877-5 mg), Resiquimod (cat# SML0196-10 mg), theophylline (cat# T1633), tetracycline (cat# 87128-25G), caffeine (cat# C0750-100G), and neomycin (cat# N1876-25G) were purchased from Millipore Sigma (Burlington, MA, USA). (6R,S)-5-formyl-5,6,7,8-tetrahydro folic acid, calcium salt (cat# 16.220-5) was purchased from Schircks Laboratories (Bauma, Switzerland). Gibco Dulbecco's Modified Eagle Medium (DMEM), Gibco antibiotic-antimycotic (100X), Gibco trypsin, Gibco fetal-bovine serum (FBS, cat# A3160702), Gibco PBS, and Lipofectamine-3000 (cat# L3000015) were purchased from Fisher Scientific. No unexpected or unusually high safety hazards were encountered.

Genetically encoded aptamer biosensor construction

A custom-made plasmid, compatible for expression in zebrafish was designed and assembled for use as the backbone vector (core plasmid) for biosensor insertion. The plasmid was sequenced verified at Plasmidsaurus. Each aptamer construct was produced via overlap extension PCR, purified, and assembled into the linearized plasmid in the 3'-UTR of GFP at the XmaI restriction site using Gibson assembly (see **Figure S1**). The Gibson mix was then transformed into competent TOP10 *E. coli* and cultured overnight at 37 °C. Colonies were picked, grown, purified, and sequence verified by Sanger sequencing using forward and reverse sequencing primers (**Table S1**).

Cell culture and transfection

Human embryonic kidney (HEK293T) cells were cultured in DMEM supplemented with 10% FBS and 1% antibiotic (penicillin and streptomycin)-antimycotic. The cells were cultured at 37 °C in a humid

atmosphere with 5% CO_2. 2×10^5 cells were seeded in each well of a 24-well plate. After 24 h, the cells were treated with drug and transfected with 0.5 μg of biosensor plasmid using Lipofectamine-3000.

Measuring single-cell biosensor response

After 72 h of incubation, cells were detached from the culture dish by incubating with trypsin for 3 min. DMEM was then added and the cells were transferred to an Eppendorf tube. The tubes were centrifuged, then the media was removed and replaced by PBS supplemented with 1% BSA. 20,000 cells from each sample were analyzed using the BD Accuri C6 plus Flow Cytometer with the corresponding filters for GFP (ex/em: 488/510 nm) and mCherry (ex/em: 587/610 nm). Data were processed and analyzed using the standard software package FlowJo (Mac version 10.8.1; FlowJo). Specifically, data were first converted into a FlowJo-compatible format (FCS3.1). Then, viable cells were isolated through two consecutive gates: 1) Scatter gate: side scatter (log) vs. forward scatter (linear); 2) Singlet gate: height vs. area of forward scatter (linear). The median EGPF level for an isolated group of viable cells under each experimental condition was exported and plotted in GraphPad Prism (v8.4.3). Each experiment was done in triplicate. The error bars represent the standard deviation for the three replicates. The limit of detection (LOD) was calculated using the following equation:[93]

$$LOD = 3.3 \times (Standard\ deviation\ of\ background)/Slope \quad (1)$$

Live cell imaging

2×10^5 cells were seeded in each well of a 24-well plate. After 24 h, the cells were transfected with 0.5 μg of the appropriate biosensor-contained plasmid using Lipofectamine-3000. After 48 h, cells were analyzed by Evos light microscopy using the 40X objective. Fluorescence of GFP (ex/em: 488/510 nm) and mCherry (ex/em: 587/610 nm) were imaged, respectively.

Zebrafish husbandry

Zebrafish [WT AB (ZL1) and Casper (ZL1714)] were purchased from the Zebrafish International Resource Center (ZIRC). Adults were maintained at 28.5°C in a recirculating system (Iwaki Aquatics) on a 14:10 h light:dark cycle and fed in the morning with Ziegler's adult zebrafish diet and in the afternoon with brine shrimp. Embryos were obtained through natural mating and cultured at 28–30 °C in E3 medium. Embryos were staged as described previously.[94] All zebrafish larvae were raised on a rotifer/brine shrimp diet starting at 5 days post fertilization (dpf) unless otherwise indicated. The IACUC committee at East Carolina University approved all animal procedures (AUP#W262).

Testing the toxicity of small molecule drugs in zebrafish

A 25 mM stock solution of theophylline was prepared in E3 medium. The fish were loaded into a 6-well plate and imaged 2 h post dosage (hpd), 4 hpd, 8 hpd, and 24 hpd. Each well in the 6-well plate had approximately 45 fish per well. Three dosages of drug (0.5 mM, 1 mM, and 2 mM) were used alongside an untreated control group. The wells that housed the fish were filled with 11 mL of E3 buffer and dosed with an amount of drug appropriate for the target concentration. The 6-well plate was then stored in an incubator set to 28° C. At each chosen timepoint, 10 fish were removed and imaged. Total body length was then measured using Olympus cellSens software. Values were recorded in an Excel spreadsheet.

Transgenic zebrafish

Transgenic zebrafish were generated using Tol2-mediated transgenesis.[75, 86] Plasmid DNA and Tol2 mRNA were premixed and co-injected into one-cell-stage WT embryos (50 pg of plasmid; 50 pg of mRNA). Fish were raised to adulthood and mated with Casper fish to identify founders with germline transmission. The resulting F1 embryos were again outcrossed to Casper fish and a single F2 adult for each line was used to generate embryos for this study.

Zebrafish imaging and fluorescence intensity quantification for zebrafish measurements

Live larvae were mounted laterally on a glass slide using 1.0% low melting point agarose. Larvae were imaged on a Leica M165 equipped with a Flexacam C3 Color CMOS camera. Images were saved as TIFFs and imported into FIJI. Pixel intensities were quantified in FIJI by using the polygon tool on the bright-field image to circumscribe the trunk of the zebrafish. The average fluorescence intensity within the same region of the corresponding fluorescent micrograph was reported. Values were exported to an Excel spreadsheet, wherein background pixel intensity from above the trunk region were subtracted and the GFP/mCherry ratio calculated.

Statistics of zebrafish experiments

Embryos from each mating were randomly distributed across tested conditions, and unfertilized and developmentally abnormal embryos were removed prior to compound treatment. No statistical methods were used to determine sample size per condition. Values for individual fish are plotted, and each distribution was assessed using the Shapiro-Wilk test and determined to be normally distributed.

ASSOCIATED CONTENT

All data supporting the findings of this study are available in the main text or the supplementary materials.

AUTHOR INFORMATION

Corresponding author

Maureen McKeague – Department of Pharmacology and Therapeutics, Faculty of Medicine and Health Sciences, McGill University, Montreal, QC, H3G 1Y6, Canada. Department of Chemistry, Faculty of Science, McGill University, Montreal H3A 0B8, QC, Canada; Email: maureen.mckeague@mcgill.ca

Authors

Eiman A. Osman - Department of Chemistry, Faculty of Science, McGill University, Montreal H3A 0B8, QC, Canada; Email: eiman.osman@mcgill.ca

Thomas P. Rynes - Department of Pharmacology and Toxicology, Brody School of Medicine, East Carolina University, Greenville 27834, NC, US; Email: rynest23@ecu.edu

Lucia Wang - Department of Pharmacology and Therapeutics, Faculty of Medicine and Health Sciences, McGill University, Montreal, QC, H3G 1Y6, Canada; Email: lucia.wang@mail.mcgill.ca

Karen Mruk - Department of Pharmacology and Toxicology, Brody School of Medicine, East Carolina University, Greenville 27834, NC, US; Email: mrukk23@ecu.edu

Author contributions

M. M. and K. M. conceived the idea and designed the research. E. A. O., T. R. and L. W. performed the experiments and analyzed the data. E. A. O. and M. M. wrote the manuscript. All the authors approved the final version of the manuscript.

ACKNOWLEDGEMENTS

The research was financially supported by grants from National Institutes of Health (GM143565 to K.M. and M.M.); National Science and Engineering Research Council of Canada (Discovery Grant to M.M); the Canada Foundation for Innovation (JELF for equipment to M.M), the Fonds de Recherche Nature et Technologies (Établissement de la relève professorale to M.M). We are grateful to members of the McKeague and Mruk labs for useful discussions. Thanks to Janeva Shahi and Olivia Kovecses for helping set up the assays. Special thanks to Dr. Maira Rivera for the help with figures, elements of each were created with Biorender (with appropriate academic licensing). We thank Prof. Nathan Luedtke for revising the manuscript. We also thank Prof. Nathan Luedtke and Kaifeng Zhao for help with microscopy.

REFERENCES

1. Chu, X.; Korzekwa, K.; Elsby, R.; Fenner, K.; Galetin, A.; Lai, Y.; Matsson, P.; Moss, A.; Nagar, S.; Rosania, G. R.; Bai, J. P. F.; Polli, J. W.; Sugiyama, Y.; Brouwer, K. L. R.; Consortium, I. T., Intracellular Drug Concentrations and Transporters: Measurement, Modeling, and Implications for the Liver. *Clinical Pharmacology & Therapeutics* **2013,** *94* (1), 126-141.

2. Zhao, Y.; Shen, Y.; Wen, Y.; Campbell, R. E., High-Performance Intensiometric Direct- and Inverse-Response Genetically Encoded Biosensors for Citrate. *ACS Cent Sci* **2020,** *6* (8), 1441-1450.

3. Chen, F.; Zhao, Y.; Pan, Y.; Xue, X.; Zhang, X.; Kumar, A.; Liang, X.-J., Synergistically Enhanced Therapeutic Effect of a Carrier-Free HCPT/DOX Nanodrug on Breast Cancer Cells through Improved Cellular Drug Accumulation. *Molecular Pharmaceutics* **2015,** *12* (7), 2237-2244.

4. McGhee, C. E.; Yang, Z.; Guo, W.; Wu, Y.; Lyu, M.; DeLong, C. J.; Hong, S.; Ma, Y.; McInnis, M. G.; O'Shea, K. S.; Lu, Y., DNAzyme-Based Lithium-Selective Imaging Reveals Higher Lithium Accumulation in Bipolar Disorder Patient-Derived Neurons. *ACS Cent Sci* **2021,** *7* (11), 1809-1820.

5. Daumar, P.; Dufour, R.; Dubois, C.; Penault-Llorca, F.; Bamdad, M.; Mounetou, E., Development and validation of a high-performance liquid chromatography method for the quantitation of intracellular PARP inhibitor Olaparib in cancer cells. *J Pharm Biomed Anal* **2018,** *152*, 74-80.

6. Mutuku, S. M.; Trim, P. J.; Prabhala, B. K.; Irani, S.; Bremert, K. L.; Logan, J. M.; Brooks, D. A.; Stahl, J.; Centenera, M. M.; Snel, M. F.; Butler, L. M., Evaluation of Small Molecule Drug Uptake in Patient-Derived Prostate Cancer Explants by Mass Spectrometry. *Scientific Reports* **2019,** *9* (1), 15008.

7. Weigt, D.; Sammour, D. A.; Ulrich, T.; Munteanu, B.; Hopf, C., Automated analysis of lipid drug-response markers by combined fast and high-resolution whole cell MALDI mass spectrometry biotyping. *Scientific Reports* **2018,** *8* (1), 11260.

8. Lu, X.; Lin, B.; Xu, N.; Huang, H.; Wang, Y.; Lin, J.-M., Evaluation of the accumulation of disulfiram and its copper complex in A549 cells using mass spectrometry. *Talanta* **2020,** *211*, 120732.

9. Yuan, Y.; Zhang, J.; Qi, X.; Li, S.; Liu, G.; Siddhanta, S.; Barman, I.; Song, X.; McMahon, M. T.; Bulte, J. W. M., Furin-mediated intracellular self-assembly of olsalazine nanoparticles for enhanced magnetic resonance imaging and tumour therapy. *Nature Materials* **2019,** *18* (12), 1376-1383.

10. Wang, Y.; Hummon, A. B., Quantification of Irinotecan in Single Spheroids Using Internal Standards by MALDI Mass Spectrometry Imaging. *Analytical Chemistry* **2023,** *95* (24), 9227-9236.

11. Zhang, X.; Scalf, M.; Berggren, T. W.; Westphall, M. S.; Smith, L. M., Identification of Mammalian Cell Lines Using MALDI-TOF and LC-ESI-MS/MS Mass Spectrometry. *Journal of the American Society for Mass Spectrometry* **2006,** *17* (4), 490-499.

12. Pharmacokinetic Modeling of Paracetamol Uptake and Clearance in Zebrafish Larvae: Expanding the Allometric Scale in Vertebrates with Five Orders of Magnitude. *Zebrafish* **2016,** *13* (6), 504-510.

13. Li, R.; Qi, H.; Ma, Y.; Deng, Y.; Liu, S.; Jie, Y.; Jing, J.; He, J.; Zhang, X.; Wheatley, L.; Huang, C.; Sheng, X.; Zhang, M.; Yin, L., A flexible and physically transient electrochemical sensor for real-time wireless nitric oxide monitoring. *Nature Communications* **2020,** *11* (1), 3207.

14. Chen, R.; Gore, F.; Nguyen, Q.-A.; Ramakrishnan, C.; Patel, S.; Kim, S. H.; Raffiee, M.; Kim, Y. S.; Hsueh, B.; Krook-Magnusson, E.; Soltesz, I.; Deisseroth, K., Deep brain optogenetics without intracranial surgery. *Nature Biotechnology* **2021,** *39* (2), 161-164.

15. Cheng, C.; Chen, W.; Jin, H.; Chen, X., A Review of Single-Cell RNA-Seq Annotation, Integration, and Cell-Cell Communication. *Cells* **2023,** *12* (15).

16. Choi, J.; Li, J.; Ferdous, S.; Liang, Q.; Moffitt, J. R.; Chen, R., Spatial organization of the mouse retina at single cell resolution by MERFISH. *Nat Commun* **2023,** *14* (1), 4929.

17. Rau, K.; Rentmeister, A., Making the Message Clear: Concepts for mRNA Imaging. *ACS Cent Sci* **2017,** *3* (7), 701-707.

18. Chitnis, A.; Dalle Nogare, D., Time-lapse imaging beyond the diffraction limit. *Methods* **2018,** *150*, 32-41.

19. Shu, X., Imaging dynamic cell signaling in vivo with new classes of fluorescent reporters. *Curr Opin Chem Biol* **2020,** *54*, 1-9.

20. Amat, F.; Keller, P. J., Towards comprehensive cell lineage reconstructions in complex organisms using light-sheet microscopy. *Dev Growth Differ* **2013,** *55* (4), 563-78.

21. Veerapathiran, S.; Wohland, T., Fluorescence techniques in developmental biology. *J Biosci* **2018,** *43* (3), 541-553.

22. Foret, M. K.; Do Carmo, S.; Lincoln, R.; Greene, L. E.; Zhang, W.; Cuello, A. C.; Cosa, G., Effect of antioxidant supplements on lipid peroxidation levels in primary cortical neuron cultures. *Free Radical Biology and Medicine* **2019,** *130*, 471-477.

23. Owen, D. M.; Magenau, A.; Majumdar, A.; Gaus, K., Imaging membrane lipid order in whole, living vertebrate organisms. *Biophys J* **2010,** *99* (1), L7-9.

24. Wang, R.; Zhou, L.; Wang, W.; Li, X.; Zhang, F., In vivo gastrointestinal drug-release monitoring through second near-infrared window fluorescent bioimaging with orally delivered microcarriers. *Nature Communications* **2017,** *8* (1), 14702.

25. Selvam, S.; Kundu, K.; Templeman, K. L.; Murthy, N.; García, A. J., Minimally invasive, longitudinal monitoring of biomaterial-associated inflammation by fluorescence imaging. *Biomaterials* **2011,** *32* (31), 7785-7792.

26. Aknoun, S.; Yonnet, M.; Djabari, Z.; Graslin, F.; Taylor, M.; Pourcher, T.; Wattellier, B.; Pognonec, P., Quantitative phase microscopy for non-invasive live cell population monitoring. *Scientific Reports* **2021,** *11* (1), 4409.

27. Shi, H.; Kwok, R. T. K.; Liu, J.; Xing, B.; Tang, B. Z.; Liu, B., Real-Time Monitoring of Cell Apoptosis and Drug Screening Using Fluorescent Light-Up Probe with Aggregation-Induced Emission Characteristics. *Journal of the American Chemical Society* **2012,** *134* (43), 17972-17981.

28. Ahrens, M. B.; Orger, M. B.; Robson, D. N.; Li, J. M.; Keller, P. J., Whole-brain functional imaging at cellular resolution using light-sheet microscopy. *Nature Methods* **2013,** *10* (5), 413-420.

29. Suzuki, M.; Shindo, Y.; Yamanaka, R.; Oka, K., Live imaging of apoptotic signaling flow using tunable combinatorial FRET-based bioprobes for cell population analysis of caspase cascades. *Scientific Reports* **2022,** *12* (1), 21160.

30. Fang, X.; Zheng, Y.; Duan, Y.; Liu, Y.; Zhong, W., Recent Advances in Design of Fluorescence-Based Assays for High-Throughput Screening. *Analytical Chemistry* **2019,** *91* (1), 482-504.

31. Wang, M.; Da, Y.; Tian, Y., Fluorescent proteins and genetically encoded biosensors. *Chemical Society Reviews* **2023,** *52* (4), 1189-1214.

32. Scarabelli, S.; Tan, K. T.; Griss, R.; Hovius, R.; D'Alessandro, P. L.; Vorherr, T.; Johnsson, K., Evaluating Cellular Drug Uptake with Fluorescent Sensor Proteins. *ACS Sensors* **2017,** *2* (8), 1191-1197.

33. Mo, G. C. H.; Ross, B.; Hertel, F.; Manna, P.; Yang, X.; Greenwald, E.; Booth, C.; Plummer, A. M.; Tenner, B.; Chen, Z.; Wang, Y.; Kennedy, E. J.; Cole, P. A.; Fleming, K. G.; Palmer, A.; Jimenez, R.; Xiao, J.; Dedecker, P.; Zhang, J., Genetically encoded biosensors for visualizing live-cell biochemical activity at super-resolution. *Nature Methods* **2017,** *14* (4), 427-434.

34. Marsafari, M.; Ma, J.; Koffas, M.; Xu, P., Genetically-encoded biosensors for analyzing and controlling cellular process in yeast. *Current Opinion in Biotechnology* **2020,** *64*, 175-182.

35. Kim, H.; Ju, J.; Lee, H. N.; Chun, H.; Seong, J., Genetically Encoded Biosensors Based on Fluorescent Proteins. *Sensors* **2021,** *21* (3), 795.

36. Paul, D.; Kales, S. C.; Cornwell, J. A.; Afifi, M. M.; Rai, G.; Zakharov, A.; Simeonov, A.; Cappell, S. D., Revealing β-TrCP activity dynamics in live cells with a genetically encoded biosensor. *Nature Communications* **2022,** *13* (1), 6364.

37. Burgstaller, S.; Bischof, H.; Rauter, T.; Schmidt, T.; Schindl, R.; Patz, S.; Groschup, B.; Filser, S.; van den Boom, L.; Sasse, P.; Lukowski, R.; Plesnila, N.; Graier, W. F.; Malli, R., Immobilization of Recombinant Fluorescent Biosensors Permits Imaging of Extracellular Ion Signals. *ACS Sensors* **2021,** *6* (11), 3994-4000.

38. Miyawaki, A.; Niino, Y., Molecular spies for bioimaging--fluorescent protein-based probes. *Mol Cell* **2015,** *58* (4), 632-43.

39. Mi, L.; Yu, Q.; Karunanayake Mudiyanselage, A.; Wu, R.; Sun, Z.; Zheng, R.; Ren, K.; You, M., Genetically Encoded RNA-Based Bioluminescence Resonance Energy Transfer (BRET) Sensors. *ACS Sens* **2023,** *8* (1), 308-316.

40. Mishra, K.; Fuenzalida-Werner, J. P.; Pennacchietti, F.; Janowski, R.; Chmyrov, A.; Huang, Y.; Zakian, C.; Klemm, U.; Testa, I.; Niessing, D.; Ntziachristos, V.; Stiel, A. C., Genetically encoded photoswitchable molecular sensors for optoacoustic and super-resolution imaging. *Nature Biotechnology* **2022,** *40* (4), 598-605.

41. Bischof, H.; Rehberg, M.; Stryeck, S.; Artinger, K.; Eroglu, E.; Waldeck-Weiermair, M.; Gottschalk, B.; Rost, R.; Deak, A. T.; Niedrist, T.; Vujic, N.; Lindermuth, H.; Prassl, R.; Pelzmann, B.; Groschner, K.; Kratky, D.; Eller, K.; Rosenkranz, A. R.; Madl, T.; Plesnila, N.; Graier, W. F.; Malli, R., Novel genetically encoded fluorescent probes enable real-time detection of potassium in vitro and in vivo. *Nat Commun* **2017,** *8* (1), 1422.

42. Chen, Z.; Zhang, S.; Li, X.; Ai, H.-w., A high-performance genetically encoded fluorescent biosensor for imaging physiological peroxynitrite. *Cell Chemical Biology* **2021,** *28* (11), 1542-1553.e5.

43. Keller, J. P.; Marvin, J. S.; Lacin, H.; Lemon, W. C.; Shea, J.; Kim, S.; Lee, R. T.; Koyama, M.; Keller, P. J.; Looger, L. L., In vivo glucose imaging in multiple model organisms with an engineered single-wavelength sensor. *Cell Reports* **2021,** *35* (12), 109284.

44. Sun, F.; Zeng, J.; Jing, M.; Zhou, J.; Feng, J.; Owen, S. F.; Luo, Y.; Li, F.; Wang, H.; Yamaguchi, T.; Yong, Z.; Gao, Y.; Peng, W.; Wang, L.; Zhang, S.; Du, J.; Lin, D.; Xu, M.; Kreitzer, A. C.; Cui, G.; Li, Y., A Genetically Encoded Fluorescent Sensor Enables Rapid and Specific Detection of Dopamine in Flies, Fish, and Mice. *Cell* **2018,** *174* (2), 481-496.e19.

45. Yoshida, T.; Nakajima, H.; Takahashi, S.; Kakizuka, A.; Imamura, H., OLIVe: A Genetically Encoded Fluorescent Biosensor for Quantitative Imaging of Branched-Chain Amino Acid Levels inside Single Living Cells. *ACS Sensors* **2019,** *4* (12), 3333-3342.

46. Cambronne, X. A.; Stewart, M. L.; Kim, D.; Jones-Brunette, A. M.; Morgan, R. K.; Farrens, D. L.; Cohen, M. S.; Goodman, R. H., Biosensor reveals multiple sources for mitochondrial NAD^+. *Science* **2016,** *352* (6292), 1474-7.

47. Alsaafin, A.; McKeague, M., Functional nucleic acids as in vivo metabolite and ion biosensors. *Biosens Bioelectron* **2017,** *94*, 94-106.

48. Wang, Y. H.; Wei, K. Y.; Smolke, C. D., Synthetic biology: advancing the design of diverse genetic systems. *Annu Rev Chem Biomol Eng* **2013,** *4*, 69-102.

49. Karloff, D. B.; Heemstra, J. M., Sweet sensation: Developing a single-cell fluorescent reporter of glycolytic heterogeneity. *Cell Chem Biol* **2021,** *28* (11), 1539-1541.

50. Chamorro-Garcia, A.; Gerson, J.; Flatebo, C.; Fetter, L.; Downs, A. M.; Emmons, N.; Ennis, H. L.; Milosavic, N.; Yang, K.; Stojanovic, M.; Ricci, F.; Kippin, T. E.; Plaxco, K. W., Real-Time, Seconds-Resolved Measurements of Plasma Methotrexate In Situ in the Living Body. *ACS Sens* **2023,** *8* (1), 150-157.

51. Su, Y.; Xu, H.; Chen, Y.; Qi, J.; Zhou, X.; Ge, R.; Lin, Z., Real-time and label-free detection of bisphenol A by an ssDNA aptamer sensor combined with dual polarization interferometry. *New Journal of Chemistry* **2018,** *42* (4), 2850-2856.

52. McKeague, M.; De Girolamo, A.; Valenzano, S.; Pascale, M.; Ruscito, A.; Velu, R.; Frost, N. R.; Hill, K.; Smith, M.; McConnell, E. M.; DeRosa, M. C., Comprehensive Analytical Comparison of

Strategies Used for Small Molecule Aptamer Evaluation. *Analytical Chemistry* **2015,** *87* (17), 8608-8612.

53. Chen, Z.-m.; Wang, Y.; Du, X.-y.; Sun, J.-J.; Yang, S., Temperature-Alternated Electrochemical Aptamer-Based Biosensor for Calibration-Free and Sensitive Molecular Measurements in an Unprocessed Actual Sample. *Analytical Chemistry* **2021,** *93* (22), 7843-7850.

54. Guo, W.; Zhang, C.; Ma, T.; Liu, X.; Chen, Z.; Li, S.; Deng, Y., Advances in aptamer screening and aptasensors' detection of heavy metal ions. *Journal of Nanobiotechnology* **2021,** *19* (1), 166.

55. Ellington, A. D.; Szostak, J. W., In vitro selection of RNA molecules that bind specific ligands. *Nature* **1990,** *346* (6287), 818-822.

56. Ricci, F.; Vallée-Bélisle, A.; Simon, A. J.; Porchetta, A.; Plaxco, K. W., Using Nature's "Tricks" To Rationally Tune the Binding Properties of Biomolecular Receptors. *Accounts of Chemical Research* **2016,** *49* (9), 1884-1892.

57. Tuerk, C.; Gold, L., Systematic Evolution of Ligands by Exponential Enrichment: RNA Ligands to Bacteriophage T4 DNA Polymerase. *Science* **1990,** *249* (4968), 505-510.

58. Groff, K.; Brown, J.; Clippinger, A. J., Modern affinity reagents: Recombinant antibodies and aptamers. *Biotechnology Advances* **2015,** *33* (8), 1787-1798.

59. Yüce, M.; Ullah, N.; Budak, H., Trends in aptamer selection methods and applications. *Analyst* **2015,** *140* (16), 5379-99.

60. Ilgu, M.; Nilsen-Hamilton, M., Aptamers in analytics. *Analyst* **2016,** *141* (5), 1551-1568.

61. Pastor, F., Aptamers: A New Technological Platform in Cancer Immunotherapy. *Pharmaceuticals (Basel)* **2016,** *9* (4).

62. Ruscito, A.; DeRosa, M. C., Small-Molecule Binding Aptamers: Selection Strategies, Characterization, and Applications. *Front Chem* **2016,** *4*, 14.

63. Sun, H.; Tan, W.; Zu, Y., Aptamers: versatile molecular recognition probes for cancer detection. *Analyst* **2016,** *141* (2), 403-15.

64. DeRosa, M. C.; Lin, A.; Mallikaratchy, P.; McConnell, E. M.; McKeague, M.; Patel, R.; Shigdar, S., In vitro selection of aptamers and their applications. *Nature Reviews Methods Primers* **2023,** *3* (1), 54.

65. Chen, A.; Yang, S., Replacing antibodies with aptamers in lateral flow immunoassay. *Biosensors and Bioelectronics* **2015,** *71*, 230-242.

66. Liang, J. C.; Chang, A. L.; Kennedy, A. B.; Smolke, C. D., A high-throughput, quantitative cell-based screen for efficient tailoring of RNA device activity. *Nucleic Acids Res* **2012,** *40* (20), e154.

67. Ausländer, S.; Ketzer, P.; Hartig, J. S., A ligand-dependent hammerhead ribozyme switch for controlling mammalian gene expression. *Molecular BioSystems* **2010,** *6* (5), 807-814.

68. Kennedy, A. B.; Vowles, J. V.; d'Espaux, L.; Smolke, C. D., Protein-responsive ribozyme switches in eukaryotic cells. *Nucleic Acids Res* **2014,** *42* (19), 12306-21.

69. Marschall, P.; Thomson, J. B.; Eckstein, F., Inhibition of gene expression with ribozymes. *Cell Mol Neurobiol* **1994,** *14* (5), 523-38.

70. Hammann, C.; Luptak, A.; Perreault, J.; de la Peña, M., The ubiquitous hammerhead ribozyme. *Rna* **2012,** *18* (5), 871-85.

71. Win, M. N.; Smolke, C. D., A modular and extensible RNA-based gene-regulatory platform for engineering cellular function. *Proceedings of the National Academy of Sciences* **2007,** *104* (36), 14283-14288.

72. Nelson, J. A.; Shepotinovskaya, I.; Uhlenbeck, O. C., Hammerheads Derived from sTRSV Show Enhanced Cleavage and Ligation Rate Constants. *Biochemistry* **2005,** *44* (44), 14577-14585.

73. Elowitz, M. B.; Levine, A. J.; Siggia, E. D.; Swain, P. S., Stochastic Gene Expression in a Single Cell. *Science* **2002,** *297* (5584), 1183-1186.

74. Mosimann, C.; Kaufman, C. K.; Li, P.; Pugach, E. K.; Tamplin, O. J.; Zon, L. I., Ubiquitous transgene expression and Cre-based recombination driven by the ubiquitin promoter in zebrafish. *Development* **2011,** *138* (1), 169-177.

75. Suster, M. L.; Kikuta, H.; Urasaki, A.; Asakawa, K.; Kawakami, K., Transgenesis in zebrafish with the tol2 transposon system. *Methods Mol Biol* **2009,** *561*, 41-63.

76. Raser, J. M.; O'Shea, E. K., Control of stochasticity in eukaryotic gene expression. *Science* **2004,** *304* (5678), 1811-4.

77. Townshend, B.; Xiang, J. S.; Manzanarez, G.; Hayden, E. J.; Smolke, C. D., A multiplexed, automated evolution pipeline enables scalable discovery and characterization of biosensors. *Nature Communications* **2021,** *12* (1), 1437.

78. Townshend, B.; Kennedy, A. B.; Xiang, J. S.; Smolke, C. D., High-throughput cellular RNA device engineering. *Nat Methods* **2015,** *12* (10), 989-94.

79. Xiang, J. S.; Kaplan, M.; Dykstra, P.; Hinks, M.; McKeague, M.; Smolke, C. D., Massively parallel RNA device engineering in mammalian cells with RNA-Seq. *Nature Communications* **2019,** *10* (1), 4327.

80. Luedtke, N. W.; Carmichael, P.; Tor, Y., Cellular uptake of aminoglycosides, guanidinoglycosides, and poly-arginine. *J Am Chem Soc* **2003,** *125* (41), 12374-5.

81. Thakur, S.; More, D.; Rahat, B.; Khanduja, K. L.; Kaur, J., Increased synthesis of folate transporters regulates folate transport in conditions of ethanol exposure and folate deficiency. *Mol Cell Biochem* **2016,** *411* (1-2), 151-60.

82. Emilien, G.; van Meurs, W.; Maloteaux, J. M., The dose-response relationship in phase I clinical trials and beyond: use, meaning, and assessment. *Pharmacol Ther* **2000,** *88* (1), 33-58.

83. Kijima, T.; Shimizu, T.; Nonen, S.; Furukawa, M.; Otani, Y.; Minami, T.; Takahashi, R.; Hirata, H.; Nagatomo, I.; Takeda, Y.; Kida, H.; Goya, S.; Fujio, Y.; Azuma, J.; Tachibana, I.; Kawase, I., Safe and Successful Treatment With Erlotinib After Gefitinib-Induced Hepatotoxicity: Difference in Metabolism As a Possible Mechanism. *Journal of Clinical Oncology* **2011,** *29* (19), e588-e590.

84. Albanese, S. K.; Chodera, J. D.; Volkamer, A.; Keng, S.; Abel, R.; Wang, L., Is Structure-Based Drug Design Ready for Selectivity Optimization? *Journal of Chemical Information and Modeling* **2020,** *60* (12), 6211-6227.

85. Patton, E. E.; Zon, L. I.; Langenau, D. M., Zebrafish disease models in drug discovery: from preclinical modelling to clinical trials. *Nature Reviews Drug Discovery* **2021,** *20* (8), 611-628.

86. Abe, G.; Suster, M. L.; Kawakami, K., Tol2-mediated transgenesis, gene trapping, enhancer trapping, and the Gal4-UAS system. *Methods Cell Biol* **2011,** *104*, 23-49.

87. Shannon, M., Life-threatening events after theophylline overdose: a 10-year prospective analysis. *Arch Intern Med* **1999,** *159* (9), 989-94.

88. Wei, K. Y.; Chen, Y. Y.; Smolke, C. D., A yeast-based rapid prototype platform for gene control elements in mammalian cells. *Biotechnol Bioeng* **2013,** *110* (4), 1201-10.

89. Bechu, A.; Liao, J.; Huang, C.; Ahn, C.; McKeague, M.; Ghoshal, S.; Moores, A., Cadmium-Containing Quantum Dots Used in Electronic Displays: Implications for Toxicity and Environmental Transformations. *ACS Applied Nano Materials* **2021,** *4* (8), 8417-8428.

90. Alsop, D.; Wilson, J. Y., Waterborne pharmaceutical uptake and toxicity is modified by pH and dissolved organic carbon in zebrafish. *Aquat Toxicol* **2019,** *210*, 11-18.

91. Trachman, R. J., 3rd; Autour, A.; Jeng, S. C. Y.; Abdolahzadeh, A.; Andreoni, A.; Cojocaru, R.; Garipov, R.; Dolgosheina, E. V.; Knutson, J. R.; Ryckelynck, M.; Unrau, P. J.; Ferre-D'Amare, A. R., Structure and functional reselection of the Mango-III fluorogenic RNA aptamer. *Nat Chem Biol* **2019,** *15* (5), 472-479.

92. Filonov, G. S.; Moon, J. D.; Svensen, N.; Jaffrey, S. R., Broccoli: rapid selection of an RNA mimic of green fluorescent protein by fluorescence-based selection and directed evolution. *J Am Chem Soc* **2014,** *136* (46), 16299-308.

93. Shrivastava, A.; Gupta, V., Methods for the determination of limit of detection and limit of quantitation of the analytical methods. *Chronicles of Young Scientists* **2011,** *2*, 21.

94. Kimmel, C. B.; Ballard, W. W.; Kimmel, S. R.; Ullmann, B.; Schilling, T. F., Stages of embryonic development of the zebrafish. *Dev Dyn* **1995,** *203* (3), 253-310.